

Studying the impact of multi-pass friction stir processing on microstructure and mechanical properties of low-carbon steel

Moein Moradi¹, Gholamreza Khalaj^{1*}, Gholamreza Ghaffari², Bahram Abdolmaleki²

¹Department of Engineering, Saveh Branch, Islamic Azad University, Saveh, Iran

²Arak Godazesh Company, Arak, Iran

Received 23 November 2022, received in revised form 26 February 2023, accepted 16 March 2023

Abstract

In this study, plain carbon steel (A216-WCB) was processed using a WC tool with a plunge depth of 2 mm, an advancing speed of 80 mm min⁻¹, and a rotational speed of 2800 rpm. Friction stir processing (FSP) was performed from one to three passes submerged under water at 5 °C. Field emission scanning electron microscope (FESEM) equipped with energy dispersive spectroscopy (EDS) and optical microscope (OM), Vickers microhardness (Hv), tensile and wear tests were used to characterize the FSPed samples. The initial grain size of the base metal (BM) was reduced from 25 μm to 3 and 5 μm in the stirred zone (SZ) and thermo-mechanically affected zone (TMAZ), respectively. The microhardness increased by a factor of 4.5 and 2.5 in SZ and TMAZ compared to the BM. This may be due to phase transformation (austenite to martensite) and grain size refinement according to the Hall-Petch equation. The ultimate tensile strength was improved by 23.9 % compared to BM, which may be due to increased grain boundaries that inhibit dislocation motion. The FSPed sample had 250 % more resistance to weight loss compared to BM. The increase in wear resistance may be attributed to the increase in microhardness and fine grain structures. Increasing the number of passes had the opposite effect on hardness, tensile strength, and wear resistance because the heat generated in subsequent passes leads to partial tempering of shear structures and recrystallization.

Key words: friction stir processing, phase transformation, cone valves, ball valves, cast steel, pipelines

1. Introduction

Corrosion causes a lot of annual damage in various industries, mainly in the oil, gas, and petrochemical industries. One example of corrosion is abrasive corrosion with fluid flow in valves due to collisions of solid particles [1]. There are various methods to prevent corrosion of the wedges, including the creation of a layer (cladding) with the process of gas tungsten arc welding (GTAW) and gas metal arc welding (GMAW) or the creation of metal matrix composites with ceramic reinforcements [2]. Although these methods have many advantages, they also come with many deficiencies, including fabrication cost, spraying of welding materials, and distortion due to welding operations. To solve these problems, a new method based on severe plastic deformation in the solid state

was proposed [3]. Due to a lower heat input resulting from the friction stir welding/processing (FSW/P) compared to fusion welding processes, metallurgical changes in the HAZ are expected to be reduced, and distortions and residual stresses in steels will be minimized. This issue is very important in welding thick sections (shipbuilding and heavy industries). Furthermore, due to the solid-state nature of the FSW/P, the problems related to hydrogen embrittlement in steels are solved [4–6]. It was also shown that the hardness of the SZ is much higher than that of the BM, which is compatible with the tensile strength results [7].

Due to the development of tools, the FSW technique has been extended to many harder materials, including copper alloys, titanium, nickel, and steel. Rotary tools commonly used for FSW of high melting point metals include WC-Co for welding Cu [8], Ti

*Corresponding author: e-mail address: gh.khalaj@srbiau.ac.ir

[9, 10], and steel [11], TiC base cermet for steel welding [12], Si₃N₄ ceramic for welding austenitic stainless steel containing high nitrogen [13, 14], and polycrystalline cubic boron nitride (pcBN) for welding DP980 steel [15] and nickel-based alloys [16, 17]. Various articles have been published about the FSP of steel [18–22]. Mohan et al. studied the FSW of steels in a review article [23]. Also, Merah et al. published a comprehensive literature review on the FSP/FSW of steels [24]. They discussed the influence of FSP parameters, such as advancing speed, rotational speed, tool material, etc., on steel's performance, such as microstructure, mechanical, and corrosion behavior. They concluded that FSP increases tensile strength and hardness. However, it reduces the ductility in most types of steel. Furthermore, FSP improves corrosion resistance in steels due to changes in surface compositions and the formation of stable passive films. It also enhances wear resistance and fatigue life in all types of steels due mainly to the hardened FSPed surface.

Sun et al. used the pcBN tool to make a 40 mm thick sheet of low-carbon steel plates by double-sided FSW [25]. The tool rotation speed and traveling speed were constant at 150 rpm and 25 mm min⁻¹, respectively. The microstructure of SZ consisted of a coarse acicular ferrite and bainite structure, while the TMAZ showed two types of microstructures, one containing a fine ferrite and bainite structure and another one containing a structure of mixed ferrite and pearlite. Hardness distribution and tensile tests showed that the welded area has better mechanical properties than the BM [25]. Wang et al. FSWed Q235 low carbon steel with a WC-Co stir pin consisting of a hexagonal cone-shaped needle and a cylindrical shoulder under a rotating speed of 475 rpm and a welding speed of 47.5 mm min⁻¹. The fine-grained structure, pearlite, and acicular ferrite improved the hardness and tensile strength of the joint. The ultimate tensile strength of the joint was 479 MPa, which was 1.3 % higher than the BM. However, the uniform elongation was 16 %, which showed a decrease of 33 % [26]. Yasavol et al. investigated the evolution of crystallographic texture during FSP at a constant traverse speed of 385 mm min⁻¹ and four different tool rotation rates of 400, 500, 600, and 800 rpm. They showed that according to the grain size at different tool rotation rates, dynamic recovery (DRV) occurred simultaneously with continuous dynamic recrystallization (CDRX). The dominant mechanism is grain refinement. Also, the formed textures have a more dominant effect on the mechanical properties than the grain refinement [27].

FSP has been applied to increase the surface abrasion resistance of duplex UNS S32205 steel and ASTM 743 steel [28, 29]. The processed surfaces were tested under severe pitting erosion conditions, and a significant improvement in abrasion resistance was reported for both processed materials. FSP has also been suc-

cessfully used in the processing of 1080 carbon steel, SKD61 tool steel, interstitial free (IF) steel, super-austenitic steel, AISI 420 martensitic steel, and AISI D2 tool steel [30–34]. Aldajah et al. investigated the role of FSP on the wear properties of 1080 steel. Investigations showed that the pearlite structure changed to martensite, and as a result, the hardness of the sample increased significantly. This increase improved the wear and friction behavior of steel. Then the wear behavior was investigated in two types of wear: dry wear and wear with lubrication. It was seen that in the dry state, FSP reduced the friction coefficient by 25 % and the wear rate by about 10 times, but in the lubricated state, it had a minor effect on the friction coefficient and reduced the wear rate by 4 times [30]. Chen et al. FSPed SKD61 tool steel and investigated the microstructure, tensile properties, and wear properties. As a result of FSP, fine grains with the martensitic structure were formed, which increased the hardness. The lower the heat input, the finer the grains. The width and depth of the abrasion test in the FSP sample were reduced by 62 and 86 %, respectively, compared to the original steel. Also, all the tensile samples broke from the BM. Therefore, they concluded that the production of a fine-grained martensitic structure is an effective method for creating a structure with good tensile and wear-resistant properties [31]. Singh et al. investigated the FSP on SA210 Grade A1 low-carbon steel used in boilers. The rotation speeds of tungsten carbide tools were 800 and 1400 rpm, and the processes were performed with a forward speed of 40 mm min⁻¹ in two passes. Based on the increase in tool rotation speed, the grain size decreased from 25 microns in the BM to 7.8 and 5.9 microns in the SZ, respectively. Also, the microhardness of 180 Vickers in the BM increased 1.72 and 2.38 times, respectively. They stated that the reasons for the increase in hardness and tensile strength are grain refining and phase change from austenite at the process temperature to martensite and ferrite. In another study, they were able to achieve a structure with a grain size of about 1 micron and a hardness of 2.5 times by increasing the tool rotation speed to 1900 rpm and three passes with a forward speed of 20 mm min⁻¹ [35, 36].

Sekban et al., by performing an FSP on low-carbon steel ABS-P2-96 Gr A, were able to reduce grain size from 25 to 5 microns. The rotation speed of the tungsten carbide tool was 635 rpm, and the forward speed was 45 mm min⁻¹. Tensile strength increased by 20 %, and hardness increased from 140 Vickers in the BM to 200 Vickers in the SZ. Also, the average coefficient of friction was reduced from 0.46 to 0.42, and the amount of weight loss in the wear test was reduced by half [37]. The effect of FSP on the pitting erosion properties of 13Cr4Ni steel used in water turbines was studied [29]. Microstructure studies showed that due to FSP, the microstructure was modified, and the grain size was

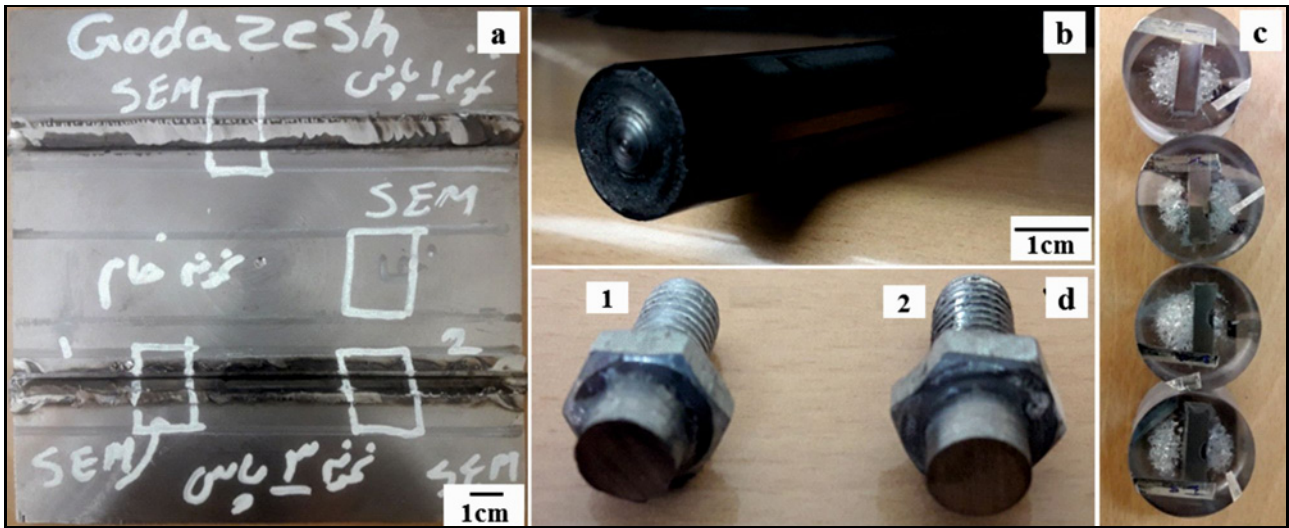


Fig. 1. (a) FSPed sample, (b) FSP tool used, (c) metallographic specimens, and (d) wear test specimens.

reduced by 10 times. Also, the size of some grains reached below $1\ \mu\text{m}$. The hardness increased by 2.6 times, and the pitting erosion resistance increased by 2.4 times. The main purpose of the present study is to apply the FSP process on plain carbon steel to modify the microstructure and evaluate changes in wear behavior. In this study, low carbon steel sheet A216-WCB was subjected to FSP submerged under water. A tungsten carbide (WC) tool was used. Structural characterizations were performed by scanning electron microscopy (SEM) and light microscopy (OM). The results show that, due to this process, the grain size was reduced, and the ferrite-pearlite phase changed to martensite. The results of hardness, tensile, and wear resistance tests show that the properties of the processed area enhanced compared to the BM.

2. Materials and methods

In the present study, in order to investigate the effects of FSP on the microstructure, tensile, micro-hardness, and wear behavior of the BM, A216-WCB cast steel (hereafter denoted as A216) in the shape of $150 \times 150 \times 6\ \text{mm}^3$ was used (Fig. 1a). Chemical composition of A216 is shown in Table 1.

The WC tool with a tool shoulder 20 mm in diameter and a conical pin with a large diameter of 7 mm, a small diameter of 5 mm, and a pin length of 2 mm was used. Figure 1b shows the worn pin after the process. During the FSP of steels, the tool and tool pin have to bear very adverse conditions and suffer considerable wear and deformation. A proper grade of WC is required for steel base material [38]. The properties of WC used in the present works were: hardness of 1300 Hv and density of $13.10\ \text{g cm}^{-3}$, as shown in Fig. 1b.

The submerged friction stir processing (SFSP) was

Table 1. Chemical composition of A216 (wt.%)

Fe	Cr	Mo	Ni	Cu	Si	Mn	C
Bal.	0.05	0.03	0.06	0.02	0.49	0.96	0.26

performed with a tool rotation speed of 2800 rpm, a transverse speed of $80\ \text{mm min}^{-1}$, a tool plunge depth of 2 mm, and a 3° tilt angle submerged under water at 5°C . The FSP was performed on the surfaces with 1 to 3 passes (so-called P1 and P3) at a similar process condition. To examine the microstructure, the cross-sections of FSPed samples were cut by a wire cut machine (Fig. 1c) and mechanically ground with 120 to 1500-grade SiC papers and were polished with 1.6 and $0.25\ \mu\text{m}$ diamond paste. Subsequently, they were etched in 2% nital solution for about 5 s. Optical microscopy and field emission scanning electron microscopy (FESEM) model TESCAN MIRA3 were used to study microstructural characterization.

The Vickers micro-hardness profiles in SZ, TMAZ, and BM were carried out on the cross-section of the samples, which was perpendicular to the traverse direction of the FSP with a load of 300 g and a dwelling time of 10 s. The micro-hardness was measured at the distance of $100\ \mu\text{m}$ below the processed surface at about $500\ \mu\text{m}$ between each measurement. The tensile tests were conducted on a universal testing machine. The BM and FSPed specimens of $6 \times 25 \times 3.8\ \text{mm}^3$ were made. Tensile tests were performed at strain rate $1 \times 10^{-3}\ \text{s}^{-1}$. Wear test was performed with a pin-on-disc device under the constant force of 80 kg, linear disc velocity of $1280\ \text{m min}^{-1}$, and applied stress of 14,500 kPa, and weight loss of each sample was measured after distances of 600, 1200, 1800, 2400, and 3000 m.

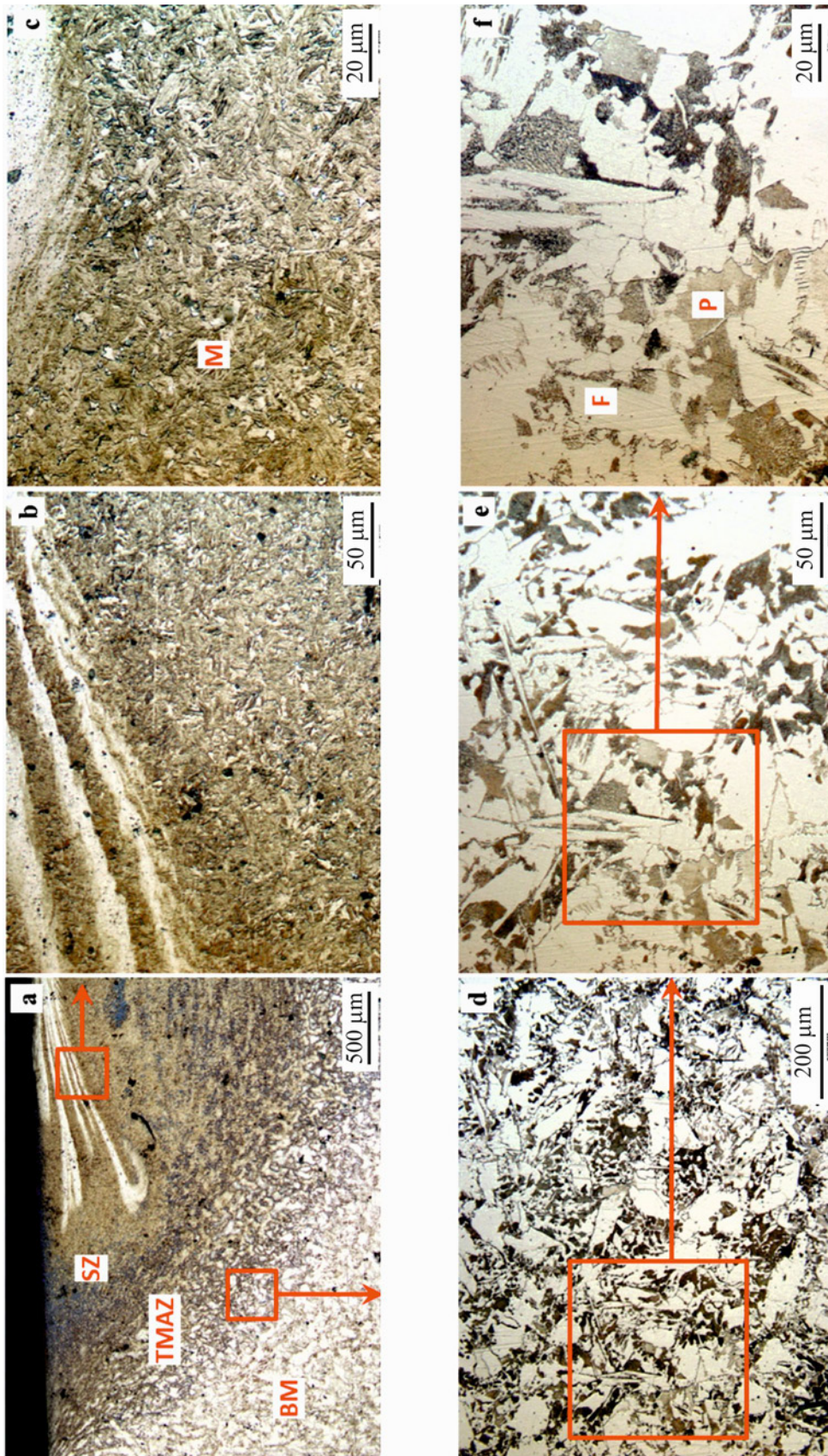


Fig. 2a–f. OM images of microstructure of base steel and FSPed samples. P1 sample: (a) general view of the FSPed area; (b) and (c) the structure of the SZ; (d), (e), and (f) the structure of the TMAZ region.

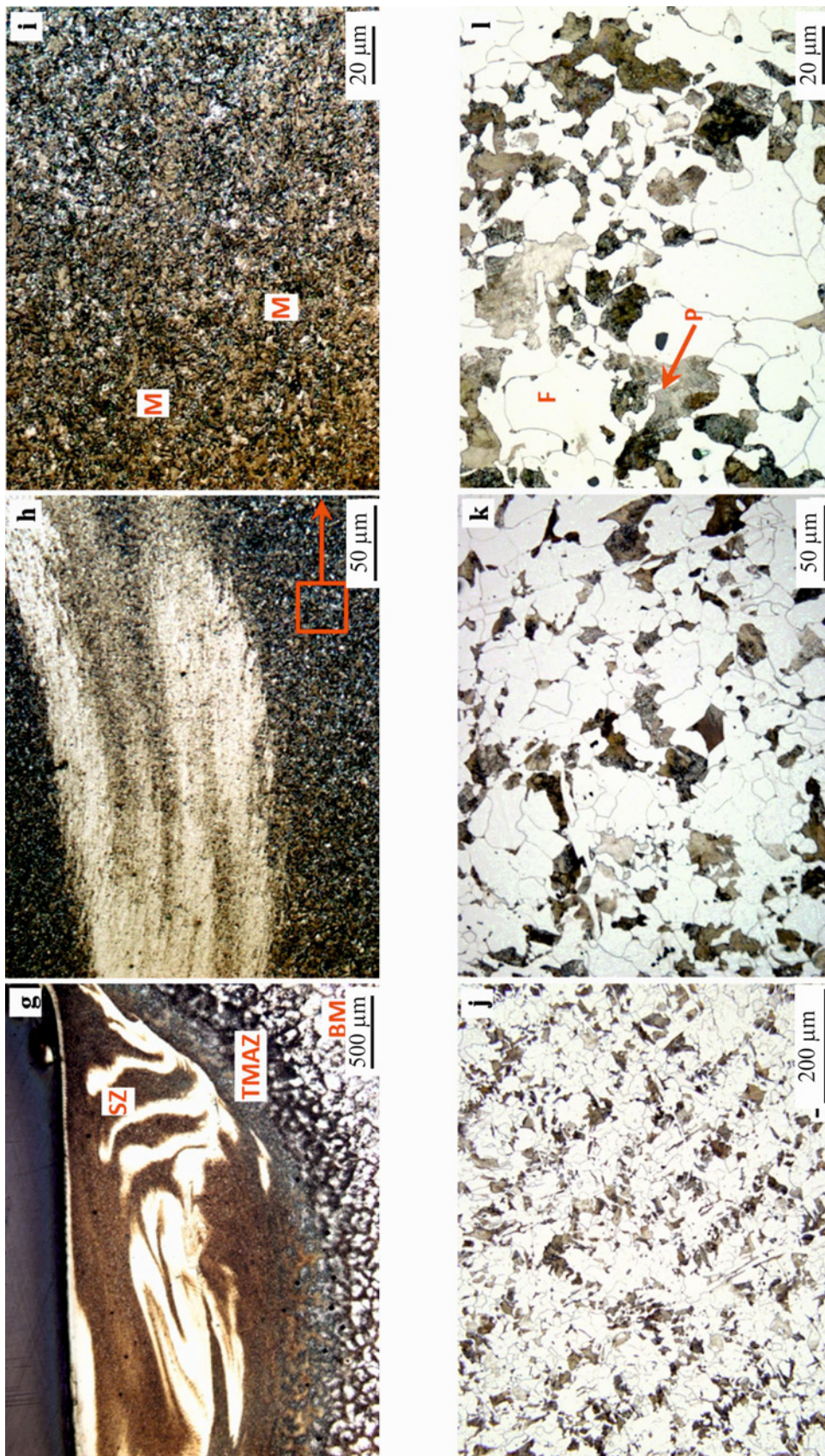


Fig. 2g-l. OM images of microstructure of base steel and FSPed samples. P3 sample: (g) general view of the FSPed area; (h) and (i) the structure of the SZ; (j), (k), and (l) the structure of the BM in different magnifications.

3. Results and discussion

3.1. Microstructure

Figure 2 shows light microscope images of base steel and FSPed samples microstructures. The FSP microstructures are usually divided and studied in two parts: the stir zone (SZ) and the thermo-mechanical affected zone (TMAZ). Figure 2a illustrates the general view of different areas of the P1 sample. Different parts of the SZ, TMAZ, and BM are named on the image. Figures 2b,c represent the structure of the SZ, identified in Fig. 2a at higher magnifications. The structure in this region consists of martensite. Figures 2d,e,f show the boundary structure of the TMAZ area and base steel with non-coaxial ferrite and pearlite structure. Figure 2g displays the general view of the different regions of the P3 sample. Figures 2h,i indicate the structure of the SZ of the P3 in higher magnifications, which includes martensite. Figures 2j,k,l demonstrate the BM structure in different magnifications. The microstructure of base steel consists of coaxial ferrite and pearlite, and with equivalent carbon of 0.44 %, the almost equilibrium structure of base steel includes 55 % pearlite and 45 % ferrite. The FSP leads to a significant modification in the microstructure, especially inside the SZ. After processing, the average grain size decreased from 25 μm in the BM to about 3 μm in the SZ. Coarse grains of ferrite and pearlite were crushed and fined under the influence of severe plastic deformation (SPD) and dynamic recrystallization (DRX) during the processing [37, 36].

Figure 3 shows scanning electron microscopy images of the SZ, TMAZ, and BM in the P1 sample at different magnifications. Figure 3a provides an overview of the area processed in the FSP; also, the SZ and the TMAZ are marked by red and yellow dashes, respectively. In Figs. 3b,c the general view of the TMAZ area is shown at different magnifications, as can be seen, part of the ferrite structure remains (Fig. 3d), while other parts have become shear structures due to temperature changes and deformation effects around the SZ (Fig. 3e). The average grain size in a TMAZ is 5 μm . Figure 3f illustrates the parts with shear structure in the TMAZ with higher magnification. Figures 3g,h,i display the shear microstructure of the SZ at different magnifications. Figures 3j,k,l demonstrate the structure of the BM at different magnifications. The structure is completely coaxial ferrite-pearlite, the amount of ferrite phase is approximately 55 %, pearlite is 45 %, and the average grain size is 25 μm .

The microstructure of TMAZ usually consists of fine, equiaxed grains that are formed as a result of DRX caused by SPD. Microscopic images in Figs. 3b–f represent the formation of various structures of ferrite,

Widmanstätten ferrite (WF), and ferrite-cementite in the TMAZ. During the process, with increasing temperature in the TMAZ, the WF structure is formed by directional ferrite plates with an aspect ratio higher than 10 : 1 at relatively low cooling rates of the austenite area. As a result of SPD in the TMAZ, DRX occurs. Thus, the structure of WF is formed with a relatively low displacement density. In the previous research, the formation of shear bands of sub-grains perpendicular to the WF plates has been observed due to SPD [38, 39]. Cementite layers in the primary microstructure pearlite are fragmented by the stirring effect of the rotating pin. Random scattering of fragmented cementite in the ferrite field in different ratios is seen in Figs. 3b–f. The formation of ferrite-cementite masses begins just before or after the onset of WF growth [39].

In Figs. 3g,h,i the structure of the SZ is shown at different magnifications. No cavities, porosity, or cracks are observed in the structure, and the structure is completely sheared. According to previous research, martensitic conversion may occur during the FSP of low-carbon or medium-carbon steels [40, 41]. On the other hand, depending on the peak temperature during the process and the cooling rate, different percentages of martensitic conversion may occur in different stirring regions with severe deformation. During the process, the SZ becomes austenitic because the peak temperature of this region is higher than A3. The austenite phase is converted to layered martensite due to rapid cooling [39]. The predominant structure of layered martensite in this area is clearly seen in the figure. The occurrence of such layered martensite during the FSP of low-carbon and medium-carbon steels has also been observed and reported in some previous studies [34, 40, 41].

Figure 4 shows SEM micrographs from different areas in the P3 sample at different magnifications. The structure of different sections (SZ, TMAZ) in the 3-pass process is not significantly different from a single pass, and the distribution and percentage of phases are almost the same. In this sample, as a result of severe deformation and an increase in dislocation density, recovery and recrystallization of the structure occur, also, due to heat input, the probability of partial tempering of the martensitic structure increases, which will be discussed in the next sections.

3.2. Microhardness

Figure 5 illustrates a comparison of the microhardness profiles of the SZ, TMAZ, and BM for P1 and P3 samples. While the hardness of the BM is 165 Vickers, by performing the FSP process, the hardness in SZ and TMAZ reaches 785 and 471 Vickers, respectively. The fineness of the grain, phase change to martensite, and increase in the density of dislocations are the

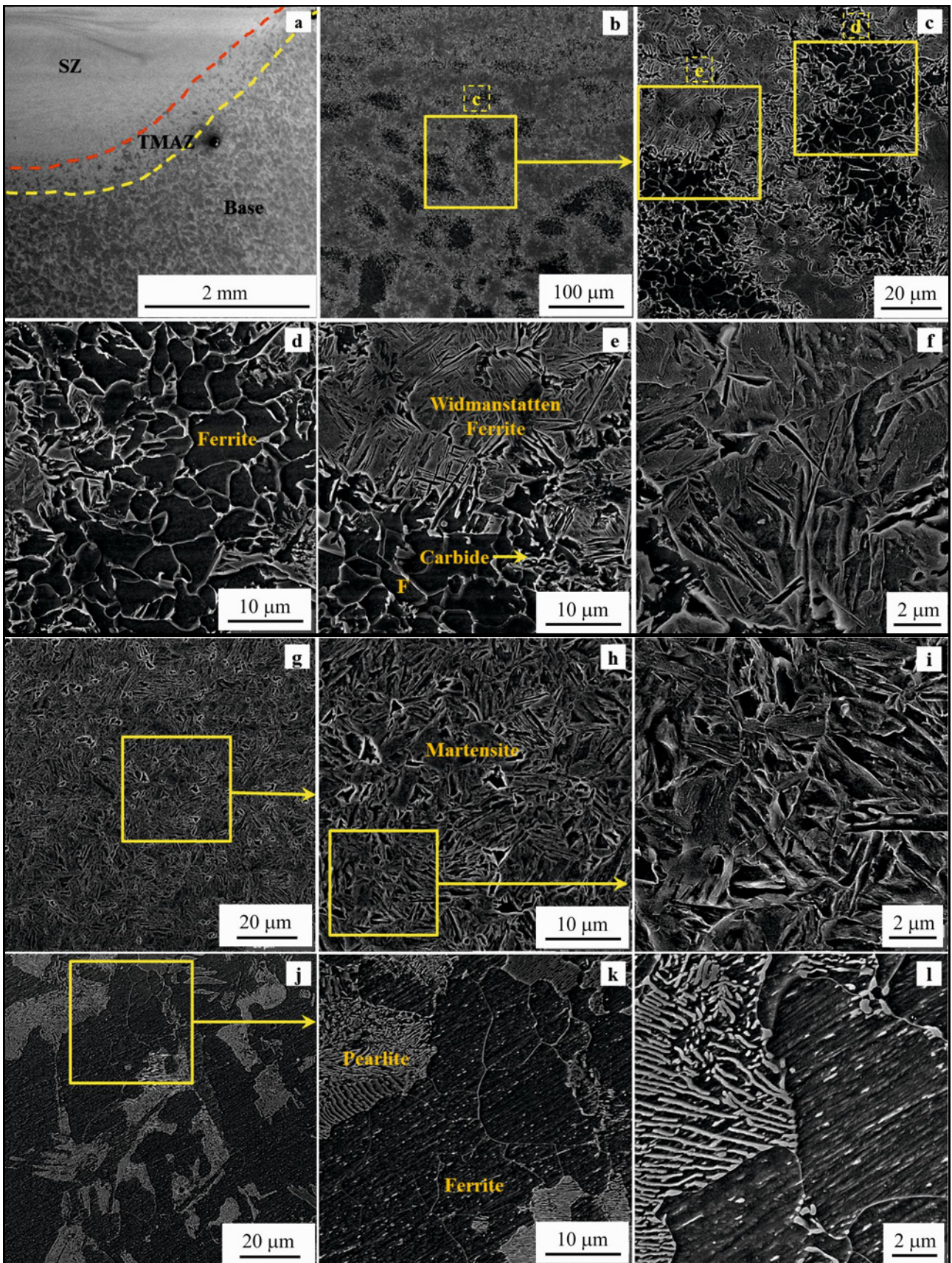


Fig. 3. SEM micrograph of P1 sample. (a) General view of the processed area; (b), (c), (d), (e), and (f) general view of the TMAZ; (g), (h), and (i) the structure of the SZ; (j), (k), and (l) the structure of the BM in different magnifications.

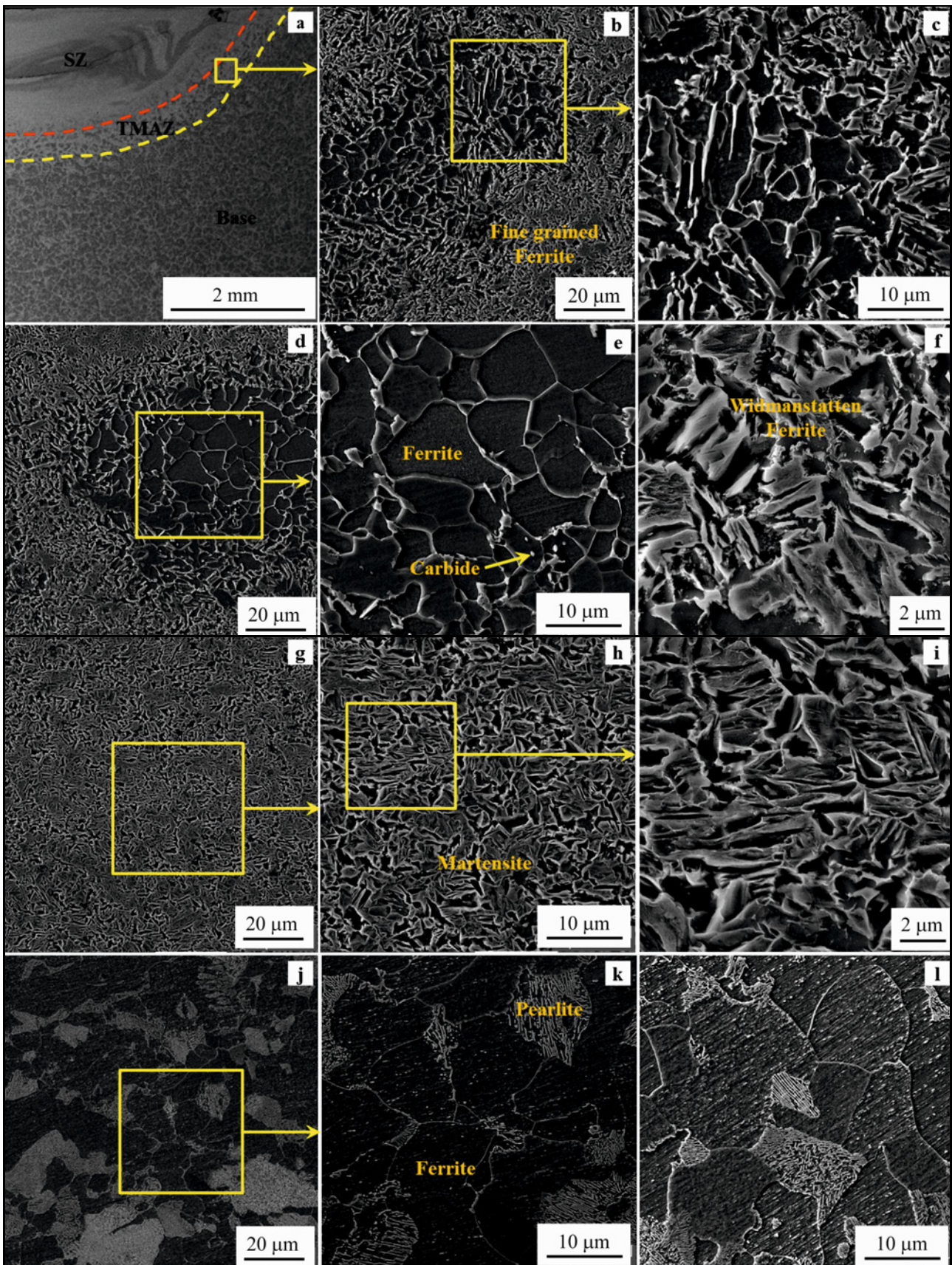


Fig. 4. SEM micrograph of P3 sample. (a) General view of the processed area; (b), (c), (d), (e), and (f) general view of the TMAZ; (g), (h), and (i) the structure of the SZ; (j), (k), and (l) the structure of the BM at different magnifications.

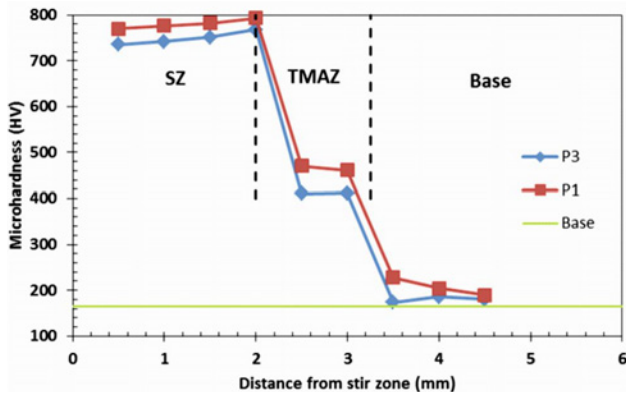


Fig. 5. Comparison of microhardness profiles of SZ, TMAZ, and BM for P1 and P3 samples.

cause of this increase of up to 4.5 times. As the distance from the center increases, the hardness diminishes in proportion to the reduction of deformation, and in TMAZ, it is 2.5 times that of the BM.

By adding the number of passes, the possibility of partial tempering of the martensite structure rises, and with recrystallization and grain growth, the hardness decreases [42]. As a result, in the P3 sample, the hardness of the SZ and the TMAZ reaches 767 and 469 HV, respectively. In this sample, in all areas, the hardness is between 30 and 40 Vickers less than that in the P1 sample. According to the Hall-Petch equation, with decreasing grain size, yield strength and hardness of the material increase. Microstructure modification may lead to a significant increase in microstructure values so that hardness is inversely related to grain size square root. Other researchers have studied the application of FSP on the surface of steels and concluded that the higher surface hardness by FSP is due to two mechanisms, mainly phase transformation and grain size reduction [43, 44]. The higher hardness in the SZ of all processed specimens may be due to the impact of the WC tool. In the present study, the reduction of grain size, phase transformation, and carbon solubility during the phase change from austenite to martensite in the SZ has led to an increase in hardness which is similar to previous studies [43, 44].

3.3. Tensile test

The Stress vs Strain graphs of the base and FSPed steel are shown in Fig. 6. It is obvious that the yield strength (YS) and ultimate tensile strength (UTS) got enhanced after FSPed for P1 and P3 samples, and ductility was reduced by significant extent for all FSPed samples. The possible rationale for the improvement of mechanical properties of FSPed samples may be recognized as the microstructural grain size modification. It has been found that the FSPed samples have moderately higher yield strength (YS) and ultimate strength (UTS) but tremendously lower elongation than the

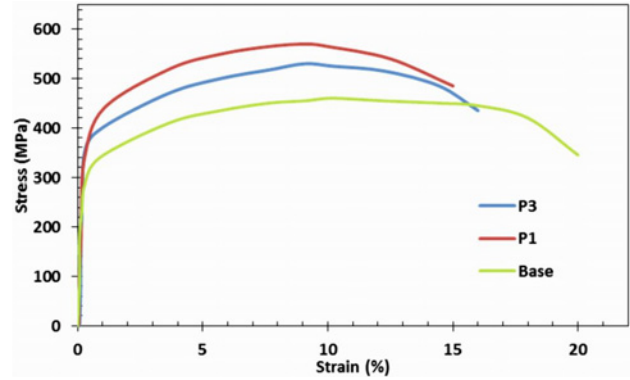


Fig. 6. Stress-strain curve for BM and FSPed samples.

parent metal. The YS and UTS showed experimental values for the BM as 283 and 462 MPa, respectively, and ductility was 20.5%. After FSP, higher YS of 310 and 302 MPa were obtained for P1 and P3 samples, respectively. Moreover, the UTS of 575 and 534 MPa were achieved in the P1 and P3 samples, respectively. As compared to BM, the ultimate tensile strength was improved by 23.9 and 15.2%, and the elongation decreased by 25.5 and 20.2% for P1 and P3 samples, respectively.

The P1 sample showed the lowest elongation and the highest strength because it had more martensite and shear structures. On the other hand, increasing the number of passes leads to a decrease in YS and UTS compared to a single pass sample and a slight increase in ductility, which corresponds to the partial tempering of the martensite structure due to the heat input of the second and third passes. In literature, similar behavior has been observed in the change of strength and ductility of FSP samples [39, 45]. The martensite phase is rapidly formed due to quenching in the stirred region, and this tendency increases with the increase of carbon percentage. The increase in hardness and strength of FSPed samples can also be attributed to the modification of the grain structure. In fact, when the grain size decreases, the grain boundary region increases. Grain boundaries prevent the movement of dislocations in the processed regions. Therefore, the increase in strength is due to the growth of the grain boundary region. A decrease in grain size leads to a decrease in ductility. In fact, stiffness-strength and elongation usually have opposite behavior. Decreasing the grain size from 25 to 3 μm reduces the effective slip space and increases the number of dislocations along the grain boundaries, i.e., when slip is delayed, the strain rate increases. A higher concentration of dislocations in SZ can lead to a change in strain hardening in the processed samples compared to the parent metal. In addition, the homogeneity of plastic deformation in fine-grained structures may also be the main reason for the slight reduction in ductility of the

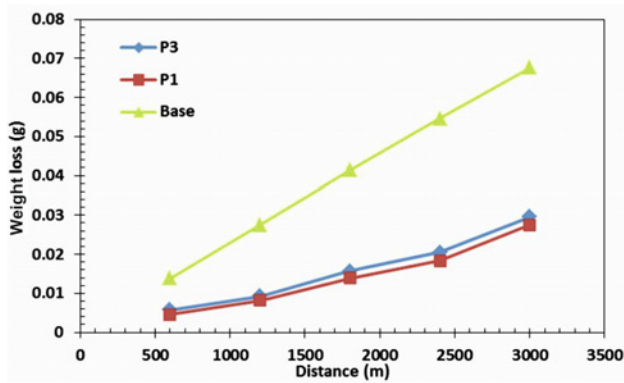


Fig. 7. Weight loss changes in terms of slip distance of BM, P1, and P3 samples.

processed samples. The smaller the grains, the lower the ability of the grain to deform, and thus the dislocation density increases. Therefore, the saturation of dislocation density in the grains of the SZ can also lead to the reduction of ductility.

3.4. Wear test

Figure 7 provides the total weight loss of the samples in terms of distance traveled in the wear test. According to this diagram, it can be seen that the weight loss values of the BM, P1, and P3 FSPed samples, after 3000 m wear distance, were measured as 67.6, 27.5, and 29.6 mg, respectively. The weight loss of the BM is about 250 % higher than that of the FSPed samples. The reason for the high weight loss of the BM sample is due to its ferrite-pearlite structure. In FSPed samples, the higher the hardness and shear structure, the lower the amount of weight loss in the wear test. The presence of the martensite phase, along with the reduction of grain size, makes an acceptable improvement in the wear rate of the FSPed sample compared to the BM sample. As previously stated, hardness and strength increased significantly after FSP, especially within the SZ. This increase in hardness increases the resistance to plastic deformation during wear and thus increases the wear resistance of the material [46, 47].

At an applied load of 80 kg-force and due to the generated heat caused by friction, adhesive bonds are formed. It is impossible to prevent the formation of adhesive bonds when the surfaces are close to each other, and on the other hand, the connection causes the unevenness of the harder material to sink into the softer material [40]. In such a situation, due to the sliding movement on the surface, the material is rocked back and forth, and this, in turn, forms scratches on the surface, which creates a mechanism of the scratch type (Fig. 8).

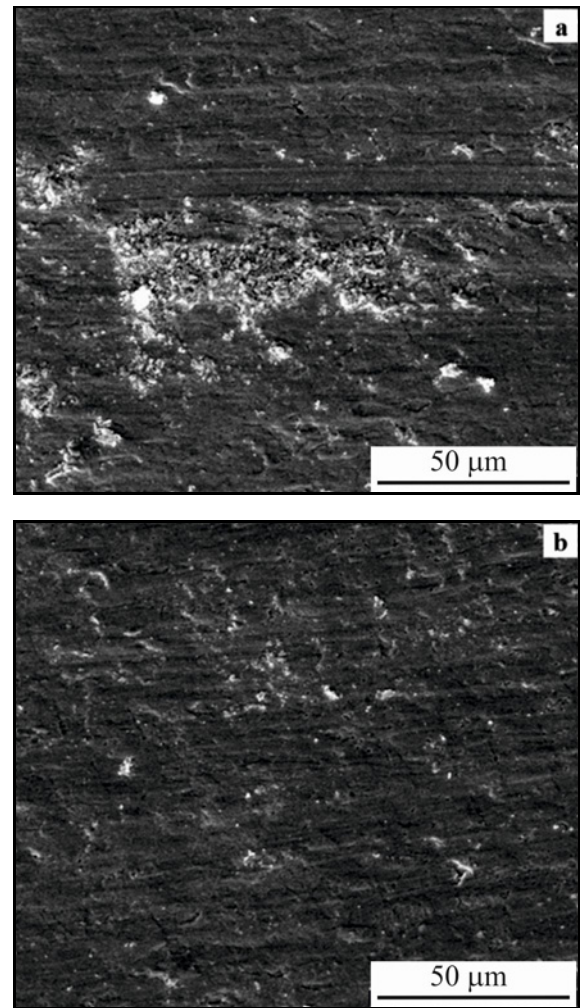


Fig. 8. SEM micrograph of the wear surface after 3000 m wear: (a) BM and (b) P1 sample.

4. Conclusions

In this research, FSP was performed on A216 cast steel sheet with a tungsten carbide tool, a rotational speed of 2800 rpm, and an advancing speed of 80 mm min^{-1} , in two modes of one pass and three passes submerged under water at 5°C . By examining the microstructure, micro-hardness, and abrasion behavior of the SZ, TMAZ, and BM, the following results were obtained:

1. The average grain size in the 1-pass sample reduced from 25 microns in BM to 3 and $5 \mu\text{m}$ in SZ and TMAZ, respectively. Grain refining in accordance with the Hall-Petch equation and the phase transformation from austenite to martensite phase increased the hardness by 4.5 and 2.5 compared to the BM.

2. By performing the FSP process, the hardness in SZ and TMAZ increased from 165 Vickers in BM to 792 and 767 Vickers, respectively. In the 3-pass FSPed sample, the hardness was between 30 and 40 Vickers less than in the 1-pass sample.

3. The YS value after FSP increased (from 283 MPa in BM) to 310 and 302 MPa for P1 and P3 samples, respectively. Also, UTS increased to 575 and 534 MPa in P1 and P3 samples compared to 462 MPa for BM. On the other hand, the percentage of length increase decreased from 20.5 to 15.2 and 16.1 %, respectively.

4. The weight loss values of BM, P1, and P3 samples after traveling a distance of 3000 m were measured as 67.6, 27.5, and 29.6 mg, respectively. The increase in wear resistance of FSPed samples was about 250 % more than that of the BM.

5. By increasing the number of passes, the hardness, wear resistance, and strength decreased to some extent with the increase in the probability of recovery of shear structures and recrystallization.

Acknowledgement

The authors would like to thank the Arak Godazesh Company for supporting this work.

References

- [1] Y. I. Oka, K. Okamura, T. Yoshida, Practical estimation of erosion damage caused by solid particle impact: Part 1: Effects of impact parameters on a predictive equation, *Wear* 259 (2005) 95–101. <http://doi.org/10.1016/j.wear.2005.01.039>
- [2] A. Neville, C. Wang, Erosion – corrosion of engineering steels – Can it be managed by use of chemicals? *Wear* 267 (2009) 2018–2026. <https://doi.org/10.1016/j.wear.2009.06.041>
- [3] W. Zhao, T. Zhang, Y. Wang, J. Qiao, Z. Wang, Corrosion failure mechanism of associated gas transmission pipeline, *Materials* 11 (2018) 1935. <http://doi.org/10.3390/ma1101935>
- [4] R. S. Mishra, Z. Y. Ma, Friction stir welding and processing, *Materials Science and Engineering R: Report* 50 (2005) 1–78. <http://doi.org/10.1007/978-3-319-07043-8>
- [5] A. P. Reynolds, W. Tang, M. Posada, J. DeLoach, Friction stir welding of DH36 steel, *Science and Technology of Welding and Joining* 8 (2003) 455–460. <http://doi.org/10.1179/136217103225009125>
- [6] N. Bhardwaj, R. Ganesh Narayanan, U. S. Dixit, M. S. J. Hashmi, Recent developments in friction stir welding and resulting industrial practices, *Advances in Materials and Processing Technologies* 5 (2019) 461–496. <http://doi.org/10.1080/2374068X.2019.1631065>
- [7] W. M. Thomas, P. L. Treadgill, E. D. Nicholas, Feasibility of friction stir welding steel, *Science and Technology of Welding and Joining* 4 (1999) 365–372. <http://doi.org/10.1179/136217199101538012>
- [8] Y. F. Sun, H. Fujii, Investigation of the welding parameter dependent microstructure and mechanical properties of friction stir welded pure copper, *Materials Science and Engineering A* 527 (2010) 6879–6886. <http://doi.org/10.1016/j.msea.2010.07.030>
- [9] H. Fujii, Y. Sun, H. Kato, K. Nakata, Investigation of welding parameter dependent microstructure and mechanical properties in friction stir welded pure Ti joints, *Materials Science and Engineering A* 527 (2010) 3386–3391. <http://doi.org/10.1016/j.msea.2010.02.023>
- [10] L. H. Wu, X. B. Hu, X. X. Zhang, Y. Z. Li, Z. Y. Ma, X. L. Ma, B. L. Xiao, Fabrication of high-quality Ti joint with ultrafine grains using submerged friction stirring technology and its microstructural evolution mechanism, *Acta Materialia* 166 (2019) 371–385. <http://doi.org/10.1016/j.actamat.2018.12.059>
- [11] L. Cui, H. Fujii, N. Tsuji, K. Nogi, Friction stir welding of a high carbon steel, *Scripta Materialia* 56 (2007) 637–640. <http://doi.org/10.1016/j.scriptamat.2006.12.004>
- [12] P. Xue, B. L. Xiao, W. G. Wang, Q. Zhang, D. Wang, Q. Z. Wang, Z. Y. Ma, Achieving ultrafine dual-phase structure with superior mechanical property in friction stir processed plain low carbon steel, *Materials Science and Engineering A* 575 (2013) 30–34. <http://doi.org/10.1016/j.msea.2013.03.033>
- [13] T. Ishikawa, H. Fujii, K. Genchi, S. Iwaki, S. Matsuoka, K. Nogi, High speed-high quality friction stir welding of austenitic stainless steel, *ISIJ International* 49 (2009) 897–901. <http://doi.org/10.2355/isijinternational.49.897>
- [14] Y. Miyano, H. Fujii, Y. Sun, Y. Katada, S. Kuroda, O. Kamiya, Mechanical properties of friction stir butt welds of high nitrogen-containing austenitic stainless steel, *Materials Science and Engineering A* 528 (2011) 2917–2921. <http://doi.org/10.1016/j.msea.2010.12.071>
- [15] N. Saunders, M. Miles, T. Hartman, Y. Hovanski, S. T. Hong, R. Steel, Joint strength in high speed friction stir spot welded DP 980 steel, *International Journal of Precision Engineering and Manufacturing* 15 (2014) 841–848. <http://doi.org/10.1007/s12541-014-0407-9>
- [16] J. Rodriguez, A. J. Ramirez, Microstructural characterisation of friction stir welding joints of mild steel to Ni-based alloy 625, *Materials Characterization* 110 (2015) 126–135. <http://doi.org/10.1016/j.matchar.2015.10.023>
- [17] S. Hanke, G. V. B. Lemos, L. Bergmann, D. Martinazzi, J. F. Dos Santos, T. R. Strohaecker, Degradation mechanisms of pcBN tool material during friction stir welding of Ni-base alloy 625, *Wear* 376 (2017) 403–408. <http://doi.org/10.1016/j.wear.2017.01.070>
- [18] A. P. Zykova, S. Y. Tarasov, A. V. Chumaevskiy, E. A. Kolubaev, A review of friction stir processing of structural metallic materials: Process, properties, and methods, *Metals* 10 (2020) 772. <https://doi.org/10.3390/met10060772>
- [19] R. G. G. R. Nandan, G. G. Roy, T. J. Lienert, T. Debroy, Three-dimensional heat and material flow during friction stir welding of mild steel, *Acta Materialia* 55 (2007) 883–895. <http://doi.org/10.1016/j.actamat.2006.09.009>
- [20] R. Ueji, H. Fujii, L. Cui, A. Nishioka, K. Kunishige, K. Nogi, Friction stir welding of ultrafine grained plain low-carbon steel formed by the martensite process, *Materials Science and Engineering A* 423 (2006) 324–330. <http://doi.org/10.1016/j.msea.2006.02.038>
- [21] L. Cui, H. Fujii, N. Tsuji, K. Nakata, K. Nogi, R. Ikeda, M. Matsushita, Transformation in stir zone of

- friction stir welded carbon steels with different carbon contents, *ISIJ International* 47 (2007) 299–306. <http://doi.org/10.2355/isijinternational.47.299>
- [22] D. H. Choi, C. Y. Lee, B. W. Ahn, J. H. Choi, Y. M. Yeon, K. Song, S. B. Jung, Frictional wear evaluation of WC-Co alloy tool in friction stir spot welding of low carbon steel plates, *International Journal of Refractory Metals and Hard Materials* 27 (2009) 931–936. <http://doi.org/10.1016/j.ijrmhm.2009.05.002>
- [23] D. G. Mohan, C. Wu, A review on friction stir welding of steels, *Chinese Journal of Mechanical Engineering* 34 (2021) 1–29. <http://doi.org/10.1186/s10033-021-00655-3>
- [24] N. Merah, M. Abdul Azeem, H. M. Abubaker, F. Al-Badour, J. Albinmousa, A. A. Sorour, Friction stir processing influence on microstructure, mechanical, and corrosion behavior of steels: A review, *Materials* 14 (2021) 5023. <http://doi.org/10.3390/ma14175023>
- [25] Y. Sun, H. Fujii, Y. Morisada, Double-sided friction stir welding of 40 mm thick low carbon steel plates using a pcBN rotating tool, *Journal of Manufacturing Processes* 50 (2020) 319–328. <http://doi.org/10.1016/j.jmapro.2019.12.043>
- [26] H. Wang, K. Wang, W. Wang, Y. Lu, P. Peng, P. Han, L. Wang, Microstructure and mechanical properties of low-carbon Q235 steel welded using friction stir welding, *Acta Metallurgica Sinica (English Letters)* 33 (2020) 1556–1570. <http://doi.org/10.1007/s40195-020-01125-w>
- [27] N. Yasavol, A. Abdollah-Zadeh, M. T. Vieira, H. R. Jafarian, Microstructure evolution and texture development in a friction stir-processed AISI D2 tool steel, *Applied Surface Science* 293 (2014) 151–159. <http://doi.org/10.1016/j.apsusc.2013.12.122>
- [28] J. D. Escobar, E. Velásquez, T. F. Santos, A. J. Ramirez, D. López, Improvement of cavitation erosion resistance of a duplex stainless steel through friction stir processing (FSP), *Wear* 297 (2013) 998–1005. <http://doi.org/10.1016/j.wear.2012.10.005>
- [29] H. S. Grewal, H. S. Arora, H. Singh, A. Agrawal, Surface modification of hydroturbine steel using friction stir processing, *Applied Surface Science* 268 (2013) 547–555. <http://doi.org/10.1016/j.apsusc.2013.01.006>
- [30] S. H. Aldajah, O. O. Ajayi, G. R. Fenske, S. David, Effect of friction stir processing on the tribological performance of high carbon steel, *Wear* 267 (2009) 350–355. <http://doi.org/10.1016/j.wear.2008.12.020>
- [31] Y. C. Chen, K. Nakata, Evaluation of microstructure and mechanical properties in friction stir processed SKD61 tool steel, *Materials Characterization* 60 (2009) 1471–1475. <http://doi.org/10.1016/j.matchar.2009.07.004>
- [32] A. Chabok, K. Dehghani, Effect of processing parameters on the mechanical properties of interstitial free steel subjected to friction stir processing, *Journal of Materials Engineering and Performance* 22 (2013) 1324–1330. <http://doi.org/10.1007/s11665-012-0424-8>
- [33] M. Mehranfar, K. Dehghani, Producing nanostructured super-austenitic steels by friction stir processing, *Materials Science and Engineering A* 528 (2011) 3404–3408. <http://doi.org/10.1016/j.msea.2011.01.016>
- [34] S. Dodds, A. H. Jones, S. Cater, Tribological enhancement of AISI 420 martensitic stainless steel through friction-stir processing, *Wear* 302 (2013) 863–877. <http://doi.org/10.1016/j.wear.2013.01.007>
- [35] S. Singh, M. Kaur, I. Saravanan, Enhanced microstructure and mechanical properties of boiler steel via Friction Stir Processing, *Materials Today: Proceedings* 22 (2020) 482–486. <http://doi.org/10.1016/j.matpr.2019.07.724>
- [36] S. Singh, M. Kaur, M. Kumar, A novel technique for surface modification of SA 210 Gr A1 steel, *Materials Today: Proceedings* 21 (2020) 1930–1936. <http://doi.org/10.1016/j.matpr.2020.01.277>
- [37] D. M. Sekban, S. M. Aktarer, H. Yanar, A. Alsarhan, G. Purcek, Improvement the wear behavior of low carbon steels by friction stir processing, In *IOP Conference Series: Materials Science and Engineering* 174 (2017) 012058. <http://doi.org/10.1088/1757-899X/174/1/012058>
- [38] A. N. Siddiquee, S. Pandey, Experimental investigation on deformation and wear of WC tool during friction stir welding (FSW) of stainless steel, *The International Journal of Advanced Manufacturing Technology* 73 (2014) 479–486. <https://doi.org/10.1007/s00170-014-5846-z>
- [39] P. Xue, B. L. Xiao, W. G. Wang, Q. Zhang, D. Wang, Q. Wang, Z. Y. Ma, Achieving ultrafine dual-phase structure with superior mechanical property in friction stir processed plain low carbon steel, *Materials Science and Engineering A* 575 (2013) 30–34. <http://doi.org/10.1016/j.msea.2013.03.033>
- [40] D. M. Sekban, S. M. Aktarer, G. Purcek, Friction stir welding of low-carbon shipbuilding steel plates: Microstructure, mechanical properties, and corrosion behavior, *Metallurgical and Materials Transactions A* 50 (2019) 4127–4140. <http://doi.org/10.1007/s11661-019-05324-8>
- [41] R. S. Mishra, Z. Y. Ma, I. Charit, Friction stir processing: A novel technique for fabrication of surface composite, *Materials Science and Engineering A* 341 (2003) 307–310. [http://doi.org/10.1016/S0921-5093\(02\)00199-5](http://doi.org/10.1016/S0921-5093(02)00199-5)
- [42] Z. W. Wang, G. N. Ma, B. H. Yu, P. Xue, G. Xie, H. Zhang, Z. Y. Ma, Improving mechanical properties of friction-stir-spot-welded advanced ultra-high-strength steel with additional water cooling, *Science and Technology of Welding and Joining* 25 (2020) 336–344. <http://doi.org/10.1080/13621718.2019.1706259>
- [43] M. I. Costa, D. Verdera, M. T. Vieira, D. M. Rodrigues, Surface enhancement of cold work tool steels by friction stir processing with a pinless tool, *Applied Surface Science* 296 (2014) 214–220. <http://doi.org/10.1016/j.apsusc.2014.01.094>
- [44] C. Lorenzo-Martin, O. O. Ajayi, Rapid surface hardening and enhanced tribological performance of 4140 steel by friction stir processing, *Wear* 332 (2015) 962–970. <http://doi.org/10.1016/j.wear.2015.01.052>
- [45] S. Singh, M. Kaur, M. Kumar, H. Singh, S. Singh, Study of microstructure evolution, mechanical properties and hot corrosion behavior of friction stir processed boiler steel, *Materials Research Express* 6 (2019) 096547. <http://doi.org/10.1088/2053-1591/ab2e48>
- [46] P. Xue, W. D. Li, D. Wang, W. G. Wang, B. Xiao, Z. Y. Ma, Enhanced mechanical properties of medium carbon steel casting via friction stir processing and

subsequent annealing, *Materials Science and Engineering A* 670 (2016) 153–158.
<http://doi.org/10.1016/j.msea.2016.06.014>

[47] M. Hajian, A. Abdollah-Zadeh, S. S. Rezaei-Nejad, H. Assadi, S. M. Hadavi, K. Chung, M. Shokouhimehr, Microstructure and mechanical properties of friction stir processed AISI 316L stainless steel, *Materials & Design* 67 (2015) 82–94.
<http://doi.org/10.1016/j.matdes.2014.10.082>